DE GRUYTER OPEN

Communications in Applied and Industrial Mathematics
ISSN 2038-0909

Research Article

Commun. Appl. Ind. Math. 7 (1), 2016, 4–22

DOI: 10.1515/caim-2016-0016

A study of the interactions between uniform and pointwise vortices in an inviscid fluid

Giorgio Riccardi*

Department of Industrial and Information Engineering,
Second University of Naples, Italy, and

CNR-INSEAN, Marine Technology Research Institute, Italy

*Email address for correspondence: giorgio.riccardi@unina2.it

Communicated by Luca Formaggia

Received on November 6, 2014. Accepted on May 18, 2015.

Abstract

The planar interactions between pair of vortices in an inviscid fluid are analytically investigated, by assuming one of the two vortices pointwise and the other one uniform. A novel approach using the Schwarz function of the boundary of the uniform vortex is adopted. It is based on a new integral relation between the (complex) velocity induced by the uniform vortex and its Schwarz function and on the time evolution equation of this function. They lead to a singular integrodifferential problem. Even if this problem is strongly nonlinear, its nonlinearities are confined inside two terms, only. As a consequence, its solution can be analytically approached by means of successive approximations. The ones at 0th (nonlinear terms neglected) and 1st (nonlinear terms evaluated on the 0-order solution) orders are calculated and compared with contour dynamics simulations of the vortex motion. A satisfactory agreement is keept for times which are small with respect to the turn-over time of the vortex pair.

Keywords: `inviscid two-dimensional vortex dynamics, uniform vortex, point vortex, contour dynamics, Schwarz function, nonlinear singular integral equation.`

AMS subject classification: `76B47, 76M40.`

1. Introduction

The planar, inviscid motion of an asymmetric pair of vortices is investigated, in the basic hypothesis that one of the two vortices is very concentrated, while the other one is rather spread. In these conditions, the dynamics of the core of the first vortex can be neglected, by schematizing it as a *point* vortex, and the second vortex can be approximated as a *uniform* one, its core being defined by a simple and closed curve, only. In this way, the motion of the pair of vortices is reduced to the dynamics of a point and of a closed curve.

The study of such kind of flow is a rather old issue in Fluid Mechanics, usually aimed to investigate the (partial) merging occurring between two co-rotating vortices. The first numerical simulations of the interactions of two vortices in an inviscid fluid dated back to the eightiess [1]. They were performed by means of a contour dynamics algorithm. Some years later, high resolution pseudo-spectral simulations of high Reynolds number interactions of two vortices (as well as a Hamiltonian, reduced model based on the dynamics of elliptical vortices [2]) were used in [3] to establish which vortex is dominant, or "victorious". In the same year, an important theoretical/experimental analysis [4] investigated the same flow in a geophysical framework.

Once the sophisticated algorithm of the *contour surgery* was developed [5], numerical simulations of asymmetric interactions (the vortices had equal vorticity, but different sizes) at extremely high Reynolds numbers [6] pointed out that complete vortex merger is very rare, while often *partial merger* occurs. Other kinds of interaction were also found: the elastic one, the partial and the complete straining-outs. Few years later, more extensive contour dynamics simulations were carrier out [7], by considering also different vorticity levels. An empirical critical merging distance was deduced, involving the ratio between the vorticity levels, too. In addition to contour dynamics (or surgery) and pseudo-spectral approaches, also the particle in cell method has been used for numerically simulating high Reynolds number interactions. As a sample, an interesting comparison between simulations and experiments (in an electron plasma) was carried out in [8] and an excellent agreement was found.

Among many others, two papers have enlightened the asymmetric merging mechanism in recent times. In the first [9], the merging has been explained in terms of rate of strain and co-rotating streamfunction, while the second one [10] uses the Lamb-Oseen vortex to build a model in surprising qualitative agreement with the numerical simulations.

More general analyses of the interactions between a point vortex and a uniform one are quite rare in literature. An intriguing model for studying the motion of point vortices inside a uniform one was built in [11], with the aim to investigate the breaking of Kelvin waves, that triggers the filamentation of the vortex boundary. By assuming the parameter $\lambda :=$ mean $|$point vortex circulations$|/$ uniform vortex circulation $\ll 1$, it is found that a "fast" (within one rotation period) filamentation occurs if one of the point vortices approaches the boundary at a distance of the order $\lambda^{0.566}$, while if all the vortices are far from the boundary, the vortex can experience a "slow" filamentation, at times of order $-(\log \lambda)/\lambda$. In the same year, an important experimental proof of this study was supplied by [12].

Experiments showed also that, for a sufficiently intense point vortex, the wave travelling on the boundary of the uniform vortex evolves into a vorticity hole within the disk (or an antivortex in a frame rotating with the vortex core).

In the present paper, the study of the vortex interactions will be approached from an analytical point of view, by extending to these flows the technique used in investigating the self-induced motion of a uniform vortex [13–15]. A novel integral relation between the Schwarz function of the boundary of the uniform vortex and the (complex) conjugate velocity , as well as an evolution equation for the same function are used to build the integrodifferential problem describing the motion. Its analytical solution is handled by means of successive approximations.

2. Set-up of the mathematical model

At the initial time ($t = 0$), the vorticity is the sum of a piecewise constant function, taking the values ω (> 0) inside a connected and bounded domain $P(0)$ and vanishing outside, and of a Dirac function of amplitude $\hat{\Gamma}$ located at the point $\boldsymbol{y}(0)$. This point will be hereafter taken outside the boundary of $P(0)$ ($\partial P(0)$. The motion is assumed planar (the plane of the motion is identified with the complex one) and the fluid isochoric and inviscid, so that the vorticity is only convected and the point vortex remains pointwise. The present paper is aimed to analytically investigate the motion of the curve $\partial P(t)$ and of the point $\boldsymbol{y}(t)$.

The conjugate velocity induced by the uniform vortex is written [16] in terms of a Cauchy integral of the *Schwarz function* $\boldsymbol{\Phi}$ of the curve $\partial P(t)$ [17]. As discussed in [15], its time evolution satisfies the equation: $(\partial_t + \boldsymbol{U}\partial_{\boldsymbol{x}})\boldsymbol{\Phi} = \overline{\boldsymbol{U}}$, where $\boldsymbol{U}$ ($\overline{\boldsymbol{U}}$) is the analytic continuation of the velocity $\boldsymbol{u}$ ($\overline{\boldsymbol{u}}$) on $\partial P(t)$. Note that the left-hand-side is just the analytic continuation of the material derivative of $\boldsymbol{\Phi}$, indicated by $D_t\boldsymbol{\Phi}$ below. The non-linear integro-differential problem (space and time dependences are omitted, for shortness)

$$
\begin{cases}
D_t\boldsymbol{\Phi} = \dfrac{\omega}{4\boldsymbol{i}}\big(\boldsymbol{\Phi} + \dfrac{1}{\pi\boldsymbol{i}} ⨍_{\partial P} d\boldsymbol{w}\,\dfrac{\boldsymbol{\Phi}}{\boldsymbol{x}-\boldsymbol{w}}\big) + \dfrac{\hat{\Gamma}}{2\pi\boldsymbol{i}}\,\dfrac{1}{\boldsymbol{x}-\boldsymbol{y}} \quad \text{for any } \boldsymbol{x} \in \partial P \\
\dot{\overline{\boldsymbol{y}}} \;= \dfrac{\omega}{4\boldsymbol{i}}\big(2\chi\overline{\boldsymbol{y}} + \dfrac{1}{\pi\boldsymbol{i}}\displaystyle\int_{\partial P} d\boldsymbol{w}\,\dfrac{\boldsymbol{\Phi}}{\boldsymbol{y}-\boldsymbol{w}}\big) \\
\boldsymbol{\Phi}(\boldsymbol{x};0) = \boldsymbol{\Phi}_0(\boldsymbol{x}) \;\text{ and }\; \boldsymbol{y}(0) = \boldsymbol{y}_0 \;\text{ given}
\end{cases}
\tag{1}
$$

follows. Hereafter, the integral with a dash means that its Cauchy principal value is taken and χ holds 1 if $\boldsymbol{y}$ lies inside P and 0 if it is external.

In order to overcome the difficulties due to the convective term in $D_t\boldsymbol{\Phi}$, the problem (1) is rewritten in Lagrangian form. First of all, a *Lagrangian*

Schwarz function $\boldsymbol{S}$ is introduced. It is obtained by means of analytic continuation of its values on $\partial P(0)$, given for any $\boldsymbol{\xi}$ on this curve by the natural relation: $\boldsymbol{S}(\boldsymbol{\xi};t) := \boldsymbol{\Phi}[\boldsymbol{x}(\boldsymbol{\xi};t);t]$. [a] Then the (nonlinear) functions

$$\begin{aligned} \boldsymbol{X}(\boldsymbol{\eta},\boldsymbol{\xi};t) &:= \partial_{\boldsymbol{\eta}} \log \frac{\boldsymbol{x}(\boldsymbol{\eta};t)-\boldsymbol{x}(\boldsymbol{\xi};t)}{\boldsymbol{\eta}-\boldsymbol{\xi}} \\ \boldsymbol{Y}(\boldsymbol{\eta};t) &:= \partial_{\boldsymbol{\eta}} \log \frac{\boldsymbol{x}(\boldsymbol{\eta};t)-\boldsymbol{y}(t)}{\boldsymbol{\eta}-\boldsymbol{y}(0)} \\ \boldsymbol{V}(\boldsymbol{\xi};t) &:= \hat{\Gamma}\left[\frac{1}{\boldsymbol{x}(\boldsymbol{\xi};t)-\boldsymbol{y}(t)} - \frac{\gamma(t)}{\boldsymbol{\xi}-\boldsymbol{y}_0}\right], \end{aligned} \tag{2}$$

are introduced. In $\boldsymbol{V}$, $\boldsymbol{\gamma}$ satisfies the constraint $\boldsymbol{\gamma}(0)=1$, so that the functions (2) vanish at $t=0$. Hereafter, $\boldsymbol{\gamma}$ is assumed 1 if the point vortex is internal to the uniform one, while it is taken as $\exp(-\boldsymbol{i}\omega t/2)$ if it is external. The Lagrangian evolution equations are non-dimensionalized [b] (non-dimensional quantities will be indicated with the same symbols) by choosing a reference length $\mathcal{L}$ (related to $P(0)$) and the reference time $4/\omega$. Finally, the equations are Laplace-transformed in time ($t \leftrightarrow \boldsymbol{\sigma}$ with $\mathrm{Re}(\boldsymbol{\sigma}) > 0$, a tilde or the symbol $\mathcal{L}[\cdot]$ indicate Laplace transforms), by accounting for the proper initial conditions. The integro-differential problem (1) becomes the integral one:

$$\begin{cases} \underbrace{(\boldsymbol{i\sigma}-1)\tilde{\boldsymbol{S}} + \dfrac{1}{\pi \boldsymbol{i}} \displaystyle\fint_{\partial P(0)} d\boldsymbol{\eta}\, \frac{\tilde{\boldsymbol{S}}}{\boldsymbol{\eta}-\boldsymbol{\xi}}}_{\boldsymbol{slS}} + \boldsymbol{nlS} = \underbrace{\boldsymbol{i}\boldsymbol{\Phi}_0}_{\boldsymbol{idS}} + \underbrace{\dfrac{\Gamma\tilde{\boldsymbol{\gamma}}}{\boldsymbol{\xi}-\boldsymbol{y}_0}}_{\boldsymbol{fS}} \\ (\boldsymbol{i\sigma}-2\chi)\tilde{\tilde{\boldsymbol{y}}} + \boldsymbol{nly} = \underbrace{\boldsymbol{i}\boldsymbol{y}_0}_{\boldsymbol{idy}} \underbrace{- \dfrac{1}{\pi \boldsymbol{i}} \displaystyle\int_{\partial P(0)} d\boldsymbol{\eta}\, \frac{\tilde{\boldsymbol{S}}}{\boldsymbol{\eta}-\boldsymbol{y}_0}}_{\boldsymbol{fy}} \end{cases} \tag{3}$$

symbols $\boldsymbol{nlS}$ and $\boldsymbol{nly}$ indicating the nonlinear terms:

$$\boldsymbol{nlS} := \frac{\mathbf{1}}{\boldsymbol{\pi i}} \int_{\boldsymbol{\partial P(0)}} \boldsymbol{d\eta}\, \widetilde{\boldsymbol{XS}} - \boldsymbol{\Gamma}\, \widetilde{\boldsymbol{Y}},\ \boldsymbol{nly} := \frac{\mathbf{1}}{\boldsymbol{\pi i}} \int_{\boldsymbol{\partial P(0)}} \boldsymbol{d\eta}\, \widetilde{\boldsymbol{VS}}. \tag{4}$$

One of the most relevant features of the system (3) is that its nonlinearities are confined inside the two terms (4). This important property opens the way to the use of successive approximations (see [18] page **84**, or [19] pages **5**, **49**), leading to analytical approximate solutions for this kind of

[a] It is worth remarking that $\boldsymbol{S}(\boldsymbol{\xi};t)$ for any $\boldsymbol{\xi}$ outside $\partial P(0)$ does not give $\boldsymbol{\Phi}[\boldsymbol{x}(\boldsymbol{\xi};t);t]$, due to the fact that the flow $\boldsymbol{\xi} \mapsto \boldsymbol{x}(\boldsymbol{\xi};t)$ is not an analytic function of $\boldsymbol{\xi}$.

[b] Instead, the circulation $\hat{\Gamma}$ is non-dimensionalized as $2\hat{\Gamma}/(\pi\mathcal{L}^2\omega) =: \Gamma$.

flows. The method consits in transforming the nonlinear system (3) in an infinite hierarchy of linear problems, the kth ($k = 0, 1, \ldots$) of which being written as:

$$\left\{\begin{array}{l} slS^{(k)} = idS + fS - nlS^{(k-1)} := M^{(k)} \\ (i\sigma - 2\chi)\,\tilde{\overline{y}}^{(k)} = idy + fy^{(k)} - nly^{(k-1)} \end{array}\right. \tag{5}$$

With this approach, nonlinear terms (nlS, nly) are evaluated at the previous level $k-1$ ($nlS^{(-1)} = 0$, $nly^{(-1)} = 0$) and considered as forcing ones. Comparisons with numerical simulations of the motion show that the solution of the kth problem (5) converges as $k \to \infty$ to the Lagrangian representation of the flow. Due to the fact that the algebraic difficulties in evaluating the solution of the problem (5) increase very rapidly with k, the 0th and 1st order solutions will be only considered. They give for the first time (to the best of the author knowledge) an analytical picture of such a kind of motion.

In order to simplify the analytical handling, it will be hereafter assumed that at $t = 0$ the uniform vortex fills a circle with center on the origin. By choosing $\mathcal{L}$ as the radius of that circle, the initial vortex boundary is just the unit circle ($\mathcal{C}$).

3. Solutions at orders 0 and 1

The problems (5) corresponding to $k = 0$ and $k = 1$ are now solved.

At the 0th order, nonlinear terms are neglected. By introducing the notations: $w_0 := 1/y_0$ and $\tau := i\,e^{-it}\sin t$, the solution (in terms of vortex boundary $x^{(0)}$, correspondig Lagrangian Schwarz function $S^{(0)}$ and point vortex position $y^{(0)}$) is:

$$\begin{gathered} x^{(0)}(\xi;t) = e^{2it}\xi + \overline{\tau}\,\frac{\Gamma w_0\,\xi}{\xi - w_0}\,, \quad S^{(0)}(\xi;t) = \frac{e^{-2it}}{\xi} - \tau\,\frac{\Gamma}{\xi - y_0} \\ y^{(0)}(t) = y_0\,e^{2it}\ \text{(internal)}\ \text{ or }\ y_0 - 2w_0\,\overline{\tau}\ \text{(external)}\,. \end{gathered} \tag{6}$$

The function $x^{(0)}(\xi;t)$ (6), as well as the corresponding 1st order one (see below), gives an approximation of the vortex boundary at time t, for ξ running on $\mathcal{C}$.

Due to the simplicity of the approximation (6), it becomes possible to investigate the singular set of the corresponding (Eulerian) Schwarz function $\Phi^{(0)}$. It is obtained in the following way. The first relation (6) is inverted, by writing ξ as a function of x (supscript "$^{(0)}$" is removed, for shortness)

$$\xi = \frac{e^{-2it}}{2}\left[\,x + w_0(e^{2it} - \Gamma\,\overline{\tau}) + R\,\right]\,, \tag{7}$$

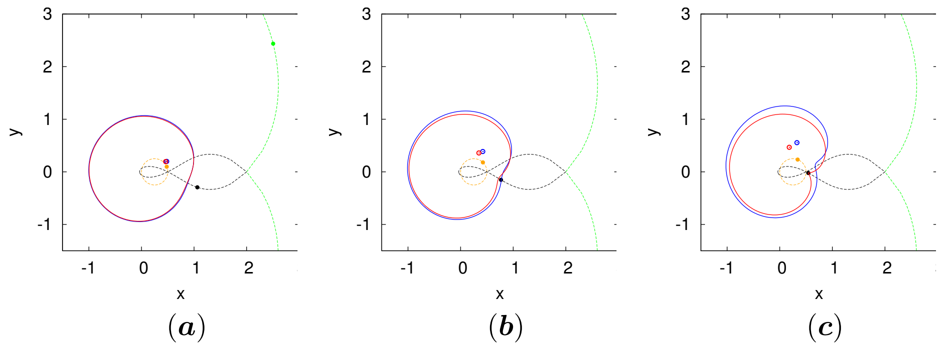

Figure 1. Trajectories of the moving pole (orange dashed line) and of the branch points (8) (x_+ green dashed, x_- black dashed) of the function (9), for $\Gamma = -3/4$ and $y_0 = 1/2$. They are superimposed to snapshots of the vortices given by the 0th order approximation (red lines and symbols) and by the numerical simulation (blue lines and symbols). Times 0.2, 0.4 and 0.6 are shown in a, b and c, respectively. Filled symbols on the trajectories indicate the singularity positions at the current time.

R being the root $[(x - x_+)(x - x_-)]^{1/2}$ having time-dependent branch points

$$x_\pm(t) = w_0 e^{2it}\left(1 \pm \sqrt{-\Gamma\,\tau}\right)^2 \ . \tag{8}$$

The function $\Phi^{(0)}$ is then obtained by inserting ξ (7) in $S^{(0)}$ (6):

$$\begin{aligned}\Phi^{(0)}(x;t) = \ & \frac{y_0 e^{-2it}}{2}\,\frac{x + w_0(e^{2it} - \Gamma\,\overline{\tau}) - R(x;t)}{x} + \\ & + \frac{\Gamma\,\tau}{2(y_0 - w_0)}\,\frac{x + w_0(e^{2it} - \Gamma\,\overline{\tau}) - 2y_0 e^{2it} - R(x;t)}{x - x^{(0)}(y_0;t)} \ .\end{aligned} \tag{9}$$

Equation (9) shows that the singular set of the 0th order (Eulerian) Schwarz function is formed by two simple poles ($x = 0$ and $x = x^{(0)}(y_0;t)$) and by two branch points (8). These latter arise from the point w_0 at $t = 0$, move at successive times as shown in the figures 1, until they collapse still on w_0 at $t = \pi$. A careful analysis of these figures suggests two important remarks: the point vortex does not coincide with a pole of $\Phi^{(0)}$ and the motion of x_- is responsible for the progressive deformation of the vortex boundary in figures 1-b and c. At the present time, the corresponding analysis for the 1st order solution is under investigation.

In order to calculate the 1st order solution, the linear approximation (6) is now used for evaluating X, Y and V (2) and then the nonlinear terms (4). The function X becomes:

$$X^{(0)} = \frac{1}{\eta - H} - \frac{1}{\eta - w_0} \ , \tag{10}$$

the simple pole H depending on the Lagrangian position ξ and on the time:

$$(11) \qquad H(\xi;t) := w_0\,\frac{\xi - w_0(1+\Gamma\tau)}{\xi - w_0} \qquad \text{with:} \quad \tau := i\,e^{-it}\sin t\,.$$

Due to the fact that the pole (11) is a linear fractional function of ξ [20], it maps $\mathcal{C}$ onto another circle, named as $\mathcal{C}_H(t)$ hereafter. It has center in $H(y_0;t) =: \Lambda(t)$ and radius $|\nu \sin t|$, with $\nu := w_0\Gamma/(w_0 - y_0)$. The algebraic structure of the 1st order solution strongly depends on the position of $\mathcal{C}_H$ with respect to $\mathcal{C}$. The center of $\mathcal{C}_H$ moves by starting at $t = 0$ from w_0 and coming back to the same point at $t = \pi$, while its radius grows in the first half-period and decreases in the second one. If certain conditions on y_0 and Γ are satisfied (see Appendix A), $\mathcal{C}_H$ intersects $\mathcal{C}$. In this case, fixed a point $\xi = e^{i\theta} \in \mathcal{C}$ and assumed $y_0 < 1$ ($y_0 > 1$), the pole (11) lies inside (outside) $\mathcal{C}$ at times $t'_H < t < t''_H$, the intersection times t'_H and t''_H depending on ξ. By naming as T'_H the minimum t'_H and as T''_H the maximum t''_H, $\mathcal{C}_H$ intersects $\mathcal{C}$ at times $T'_H < t < T''_H$ (see figure 7-a). In order to account for the relative positions of the point (11) with respect to $\mathcal{C}$, the function $\chi_H(\xi;t)$ is introduced: it holds 1 when the pole is internal to $\mathcal{C}$, while it vanishes when it lies outside. The complementary function $\chi'_H := 1 - \chi_H$ will be also used.

The evaluation on the 0th order solution (6) of Y leads to the function:

$$(12) \qquad Y^{(0)} = \frac{e^{-2it}}{\Xi_w - \Xi_y}\left(\frac{w_0 - \Xi_y}{\xi - \Xi_y} - \frac{w_0 - \Xi_w}{\xi - \Xi_w}\right) - \frac{\gamma}{\xi - y_0}\,,$$

the analytical form of the time-dependent poles Ξ_y and Ξ_w being given in Appendix B. At the initial time (and at $t = \pi$), they lie in y_0 and w_0, respectively. The analysis in Appendix B shows that for an internal point vortex ($\chi = 1$) Ξ_y lies inside $\mathcal{C}$ and Ξ_w outside at any time. On the contrary, if the point vortex is external ($\chi = 0$), Ξ_w lies inside $\mathcal{C}$ at any time, while the trajectory of Ξ_y starts and ends outside $\mathcal{C}$ and it can cross this circle, if certain conditions are satisfied. Finally, the same poles Ξ_y and Ξ_w also appear also in V:

$$(13) \qquad V^{(0)} = \frac{1}{\eta - \Xi_y} - \frac{1}{\eta - y_0} + \frac{1}{\eta - \Xi_w} - \frac{1}{\eta - w_0}\,.$$

3.1. *Point vortex outside the uniform one*

Examine now what happens if the point vortex lies inside the uniform one. Once the nonlinear terms (2) are evaluated in correspondence to the approximation (6) by using the functions (10, 12), the right hand side of the first equation in the system (5) follows as:

$$M^{(1)} = \frac{i}{\eta} + \mathcal{L}\Big[\quad 2\chi'_H\tau\left(\frac{\Gamma e^{-2it}}{\eta-\Delta} - \frac{\nu^2\tau}{\eta-\Lambda}\right) + 2y_0\chi_H\left(\nu\tau - e^{-2it}\right) + \\ + \frac{\Gamma e^{-2it}}{\Xi_w - \Xi_y}\left(\frac{w_0-\Xi_y}{\eta-\Xi_y} - \frac{w_0-\Xi_w}{\eta-\Xi_w}\right)\Big] \;,$$

in terms of the function $\Delta(t) := H(0;t) = w_0(1+\Gamma\tau)$. In correspondence to the above value of $M^{(1)}$, the solution of the singular integral equation in the system (5) leads to the 1st order Laplace transform of the Lagrangian Schwarz function:

$$\begin{aligned}\tilde{S}^{(1)} = \;& \frac{1}{\sigma+2i}\,\frac{1}{\xi} - \frac{i\Gamma}{\sigma+2i}\,\mathcal{L}\left(\frac{e^{-2it}}{\Xi_w-\Xi_y}\,\frac{w_0-\Xi_y}{\xi-\Xi_y}\right) + \\ & -\frac{i\Gamma}{\sigma}\,\mathcal{L}\left(\frac{e^{-2it}}{\Xi_y-\Xi_w}\,\frac{w_0-\Xi_w}{\xi-\Xi_w}\right) + \\ & -i\,\Sigma_+\,\mathcal{L}\left[\chi'_H\tau\left(\frac{\Gamma e^{-2it}}{\xi-\Delta} - \frac{\nu^2\tau}{\xi-\Lambda}\right) + y_0\chi_H\left(\nu\tau - e^{-2it}\right)\right] + \\ & +i\,\Sigma_-\,\mathcal{L}\left[\Gamma\,\tau\,e^{-2it}F'_\Delta - \nu^2\tau^2F'_\Lambda + y_0\left(\nu\tau - e^{-2it}\right)G_1\right]\;,\end{aligned} \tag{14}$$

where $\Sigma_\pm := 1/(\sigma+2i) \pm 1/\sigma$. The functions F'_Δ, F'_Λ and G_1 in the Laplace transform of $S^{(1)}$ are defined as:

$$\begin{aligned} F'_\Delta(\xi;t) &:= \frac{1}{\pi i}\oint_{\mathcal{C}} d\eta\,\frac{\chi'_H(\eta;t)}{(\eta-\xi)[\eta-\Delta(t)]} \\ F'_\Lambda(\xi;t) &:= \frac{1}{\pi i}\oint_{\mathcal{C}} d\eta\,\frac{\chi'_H(\eta;t)}{(\eta-\xi)[\eta-\Lambda(t)]} \\ G_1(\xi;t) &:= \frac{1}{\pi i}\oint_{\mathcal{C}} d\eta\,\frac{\chi_H(\eta;t)}{\eta-\xi} \end{aligned} \tag{15}$$

and their values depend on the relative positions of the circles $\mathcal{C}_H$ and $\mathcal{C}$. At times $t < T'$ or $t > T''$ ($\chi_H = 0$), the above functions are easily evaluated: $F'_\Delta = 1/(\xi-\Delta)$, $F'_\Lambda = 1/(\xi-\Lambda)$ and $G_1 \equiv 0$. Instead, at times $T'_H < t < T''_H$ ($\chi_H = 1$), the arc $(\eta_i, \eta_f) \subset \mathcal{C}$ is mapped by the function (11) inside $\mathcal{C}$, so that the functions (15) are evaluated by following the sketches drawn in Fig. 2 as:

$$
\begin{aligned}
F'_\Delta &= \frac{1}{\xi-\Delta}\Big(\frac{1}{\pi i}\log\frac{\eta_i-\xi}{\eta_f-\xi}+\chi'_H-\frac{1}{\pi i}\log\frac{\eta_i-\Delta}{\eta_f-\Delta}\Big)\\
F'_\Lambda &= \frac{1}{\xi-\Lambda}\Big(\frac{1}{\pi i}\log\frac{\eta_i-\xi}{\eta_f-\xi}+\chi'_H-\frac{1}{\pi i}\log\frac{\eta_i-\Lambda}{\eta_f-\Lambda}\Big)\\
G_1 &= \frac{1}{\pi i}\log\frac{\eta_f-\xi}{\eta_i-\xi}+\chi_H\,.
\end{aligned}
\tag{16}
$$

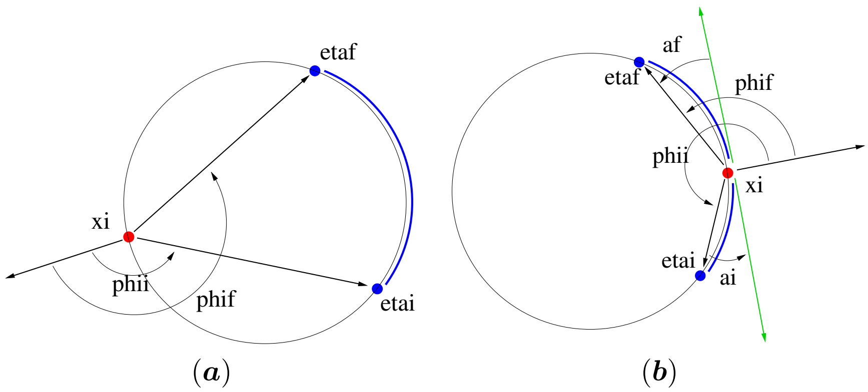

Figure 2. The domain of integration in the integrals (15) is the blue arc on $\mathcal{C}$, from η_i to η_f in counter-clockwise direction. The integrals have to be evaluated in different ways if ξ lies outside a or inside b that arc, being the Cauchy integral effective in the second case. Once a continuous branch of $\log(\eta-\xi)$ is chosen (the direction of vanishing phase is drawn with an arrow from ξ), the increment of the argument is $\varphi_f-\varphi_i$ in a and $\alpha_i+\alpha_f=\varphi_f-\varphi_i+\pi$ in b.

At times $t<T'$, the inverse Laplace transform of $\tilde{S}^{(1)}$ (14) assumes the simple form:

$$
\begin{aligned}
S^{(1)} = {} & \frac{e^{-2it}}{\xi}-2i\Gamma\int_0^t dt'\,\frac{\tau' e^{-2it'}}{\xi-\Delta}+2i\nu^2\int_0^t dt'\,\frac{\tau'^2}{\xi-\Lambda}+\\
& -i\Gamma\int_0^t dt'\,\frac{e^{-2it'}}{\Xi_y-\Xi_w}\,\frac{w_0-\Xi_w}{\xi-\Xi_w}+\\
& -i\Gamma e^{-2it}\int_0^t dt'\,\frac{1}{\Xi_w-\Xi_y}\,\frac{w_0-\Xi_y}{\xi-\Xi_y}\,,
\end{aligned}
\tag{17}
$$

while the complicated form assumed at later times will not be written here, for shortness. The (conjugate) position of the point vortex is then evaluated by solving the second equation in the system (5) and computing the inverse Laplace transform. At times $t < T'_H$ it assumes the simple form:

$$\begin{aligned}\overline{y}^{(1)} = e^{-2it}\Big[\quad & y_0(1+2it) - \frac{i\Gamma}{w_0 - y_0}\,(e^{+it}\sin t - t) + \\ & -2i\int_0^t \frac{dt'}{\Xi_w} - 2i\Gamma\int_0^t dt'\,\frac{\tau' e^{+2it'}}{y_0 - \Xi_w} + \\ & +4\Gamma\int_0^t dt'\,e^{+2it'}\int_0^{t'} dt''\,\frac{\tau'' e^{-2it''}}{y_0 - \Delta} + \\ & -4\nu^2\int_0^t dt'\,e^{+2it'}\int_0^{t'} dt''\,\frac{\tau''^2}{y_0 - \Lambda} + \\ & +2\Gamma\int_0^t dt'\,e^{+2it'}\int_0^{t'} dt''\,\frac{e^{-2it''}}{\Xi_y - \Xi_w}\,\frac{w_0 - \Xi_w}{y_0 - \Xi_w}\Big]\;.\end{aligned} \tag{18}$$

Time integrals in the **1**st order approximation (17, 18) are analytically evaluated. The building of the **1**st order approximation with the point vortex external to the uniform one is now investigated.

3.2. *Point vortex outside the uniform one*

The nonlinear term $slS^{(0)}$ (4) is evaluated in the same way and the right hand side of the first equation in the system (5) follows as:

$$\begin{aligned}M^{(1)} = \frac{i}{\eta} + \mathcal{L}\Big[\quad & 2\chi'_H\,\frac{\Gamma e^{-2it}\tau}{\eta - \Delta} + 2\chi_H\,\frac{\nu^2\tau^2}{\eta - \Lambda} + \\ & +2\chi'_H\Big(\frac{\Gamma\tau}{y_0 - w_0} + y_0 e^{-2it}\Big) + \\ & +\frac{\Gamma e^{-2it}}{\Xi_w - \Xi_y}\Big(\frac{w_0 - \Xi_y}{\eta - \Xi_y} - \frac{w_0 - \Xi_w}{\eta - \Xi_w}\Big)\Big]\;.\end{aligned}$$

The solution of the singular integral equation gives the Laplace transform of the **1**st order Lagrangian Schwarz function:

$$\begin{aligned}\tilde{S}^{(1)} = \quad & \frac{1}{\sigma + 2i}\,\frac{1}{\xi} - \frac{i\,\Gamma}{\sigma + 2i}\,\mathcal{L}\Big(\chi_y\,\frac{e^{-2it}}{\Xi_w - \Xi_y}\,\frac{w_0 - \Xi_w}{\xi - \Xi_y}\Big) + \\ & -\frac{i\,\Gamma}{\sigma}\Big[\mathcal{L}\Big(\frac{e^{-2it}}{\Xi_w - \Xi_y}\,\frac{w_0 - \Xi_w}{\xi - \Xi_y}\Big) - \mathcal{L}\Big(\frac{e^{-2it}}{\Xi_y - \Xi_w}\,\frac{w_0 - \Xi_w}{\xi - \Xi_w}\Big)\Big] + \\ & -i\,\Sigma_+\,\mathcal{L}\big[\,\Gamma\,\frac{e^{-2it}\tau\chi'_H}{\xi - \Delta} + \frac{\nu^2\tau^2\chi_H}{\xi - \Lambda} + y_0\,(\,e^{-2it} - \nu\tau\,)\,\chi'_H\,\big] + \\ & +i\,\Sigma_-\,\mathcal{L}\big[\,\Gamma e^{-2it}\tau\,F'_\Delta + \nu^2\tau^2\,F_\Lambda + y_0\,(\,e^{-2it} - \nu\tau\,)\,G'_1\,\big]\;,\end{aligned} \tag{19}$$

the new functions F_Λ and G_1' being defined as F_Λ' and G_1 in equation (15), with χ_H and χ_H' in place of χ_H' and χ_H, respectively. Their calculation is easy if the circles $\mathcal{C}_H$ and $\mathcal{C}$ do not cross: in this case, $F_\Lambda = -1/(\xi - \Lambda)$ and $G_1' = 0$. When the circles $\mathcal{C}_H$ intersects $\mathcal{C}$, these functions assume more complicated forms, similar to the ones in equation (16).

The Laplace inverse transform of $\tilde{S}^{(1)}$ (19) is evaluated at times $t < T_H'$ as:

$$
\begin{aligned}
S^{(1)} = \quad & \frac{e^{-2it}}{\xi} - 2i\nu^2 \left(\int_0^t dt' \, \frac{\chi_\Lambda' \tau'^2}{\xi - \Lambda} + e^{-2it} \int_0^t dt' \, \frac{\chi_\Lambda \tau'^2 e^{+2it'}}{\xi - \Lambda} \right) + \\
& -i\Gamma \Bigg(\int_0^t dt' \, \frac{e^{-2it'} \chi_y'}{\Xi_w - \Xi_y} \, \frac{w_0 - \Xi_y}{\xi - \Xi_y} + \\
& \qquad + e^{-2it} \int_0^t dt' \, \frac{\chi_y}{\Xi_w - \Xi_y} \, \frac{w_0 - \Xi_y}{\xi - \Xi_y} \Bigg) + \\
& -i\Gamma e^{-2it} \int_0^t \frac{dt'}{\Xi_y - \Xi_w} \, \frac{w_0 - \Xi_w}{\xi - \Xi_w} \, ,
\end{aligned}
\tag{20}
$$

while, as before, the corresponding form at later times will not be written. The 1st order point vortex trajectory is obtained by inserting $\tilde{S}^{(1)}$ (20) inside $fy^{(1)}$ and evaluating $nly^{(0)}$ by means of the function (13). At times $t < T_H'$, the Laplace inverse transform gives

$$
\begin{aligned}
\overline{y}^{(1)} = \quad & y_0 + \frac{\Gamma}{y_0 - w_0} (\tau - it) + \\
& -4\nu^2 \int_0^t dt' \, e^{-2it'} \int_0^{t'} dt'' \, \frac{\tau''^2 e^{2it''}}{y_0 - \Lambda} + \\
& -2\Gamma \int_0^t dt' \, e^{-2it'} \int_0^{t'} dt'' \, \frac{\chi_y}{\Xi_w - \Xi_y} \, \frac{w_0 - \Xi_y}{y_0 - \Xi_y} + \\
& -2\Gamma \int_0^t dt' \, e^{-2it'} \int_0^{t'} \frac{dt''}{\Xi_y - \Xi_w} \, \frac{w_0 - \Xi_w}{y_0 - \Xi_w} + \\
& +2i \Bigg(- \int_0^t dt' \, \frac{\chi_y' e^{-2it'}}{\Xi_y} + \Gamma \int_0^t dt' \, \frac{\chi_y \tau'}{y_0 - \Xi_y} + \\
& \qquad + \Gamma \int_0^t dt' \, \frac{\tau'}{y_0 - \Xi_w} \Bigg) \, .
\end{aligned}
\tag{21}
$$

Time integrals involved in the 1st order approximation (20, 21) are analytically evaluated, so that explicit formulae for the Lagrangian Schwarz function and the point vortex position are obtained.

4. Qualitative behaviour of the approximations and comparison with contour dynamics simulations

The approximations at order $\mathbf{0}$ (6) and $\mathbf{1}$ (17, 18), (20, 21) are now computed and compared with the corresponding results of contour dynamics simulations.

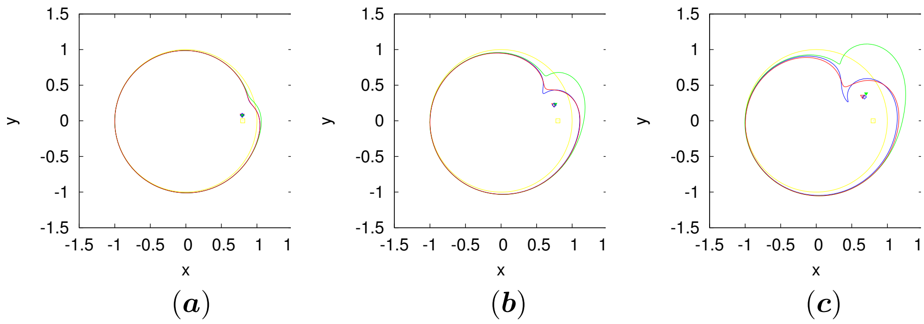

Figure 3. Boundary of the uniform vortex and point vortex position at times $t = 0.05$ a, 0.15 b, 0.25 c, for $\Gamma = 0.5$ and $y_0 = 0.8$. The results of contour dynamics simulations are drawn with blue lines and diamonds, the $\mathbf{0}$th order solution with green lines and triangles and the $\mathbf{1}$st order one with red lines and triangles. The vortices at $t = 0$ are also drawn with yellow lines and symbols. The simulations are performed with maximum errors on the area of P $-7.25 \cdot 10^{-7}$, on the first order moment (in modulus) $6.99 \cdot 10^{-7}$ and on second order moment $-6.50 \cdot 10^{-7}$.

Snapshots of the vortex motion with the point vortex inside the uniform one are shown in figures 3 (co-rotating vortices), 4 (counter-rotating). It is easily perceived that the $\mathbf{0}$th order approximation is not able to follow the vortex motion, unless during a very small initial time (see the figures 3-a, 4-a at $t = 0.05$). This behaviour is due to the fact that the $\mathbf{0}$th order approximation neglects the nonlinear terms (4), which vanish at the initial time, but become quickly important at later ones. Note also that the differences with numerical simulations are larger for the boundaries of the uniform vortex, than for the point vortex positions. The $\mathbf{1}$st order approximation substantially improves the behaviour of the $\mathbf{0}$th order one, by keeping a good agreement with the numerical simulations for larger times. Furthermore, the correspondence between approximate and numerical boundaries appears to be nonuniform. It is very good in moderate curvature regions, while it becomes worse in correspondence to the entry of irrotational fluid inside the core (see figures 3-c, 4-c), where the curvature substantially grows. One can conclude that the approximation of the nonlinear terms with $nlS^{(0)}$ and $nly^{(0)}$ prevents the $\mathbf{1}$st order boundary from following the numerical one, in high curvature regions.

Snapshots of the interactions with the point vortex outside the uniform one are drawn in figures 5 (co-rotating vortices) and 6 (counter-rotating). As in the previous cases, the 0th order approximation behaves in a quite unsatisfactoy way: its vortex boundary quickly moves away from the numerical one and also the point vortex runs on a rather different trajectory, with respect to the one obtained by means of the contour dynamics simulation. This behaviour of the 0th order point vortex is especially clear in figure 6-c. The 1st order approximation strongly improves the agreement with the numerical simulations, in terms of both vortex boundary and point vortex position. Significant differences in the boundaries appear only at later times ($t = 0.5$, figure 5-c), still in high curvature regions. Finally, note the important improvement in the point vortex position with respect to the 0th order one, in figure 6-c.

The calculation of the 1st order approximation is more complicated when the circle $\mathcal{C}_H$ crosses $\mathcal{C}$. In this case, the functions (15), F_Λ and G'_1 involve logarithms, as in the formulae (16), and time integrals have to be numerically computed. A sample case is shown in the figures 7. Times t'_H and t''_H are drawn in a vs. the argument of ξ (the times T'_H and T''_H are also indicated) and snapshots of the vortices at two consecutive times are shown in b and c. As before, the 0th order approximation behaves in a unsatisfactory way, leading to large errors in the region pushed inside the core by the point vortex. The 1st order approximation strongly improves the description of the vortex motion, even if it is not able to completely follow the above inward motion of the boundary. At the same time, it gives a satisfactory approximation of the trajectory of the point vortex.

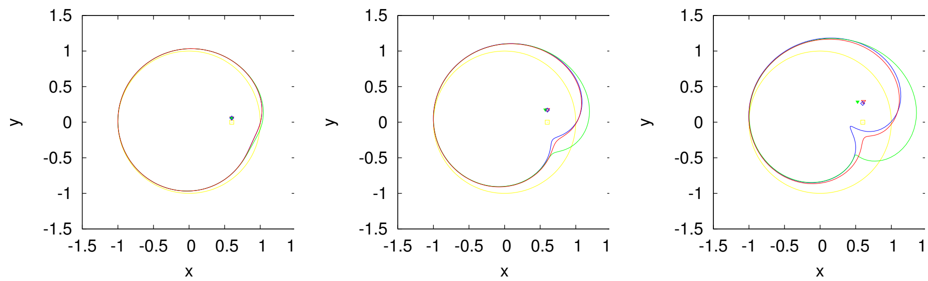

(a) (b) (c)

Figure 4. As in Fig. 3, but for $\Gamma = -1.5$ and $y_0 = 0.6$. Maximum errors are $-3.29 \cdot 10^{-7}$, $3.32 \cdot 10^{-7}$ and $-3.38 \cdot 10^{-7}$.

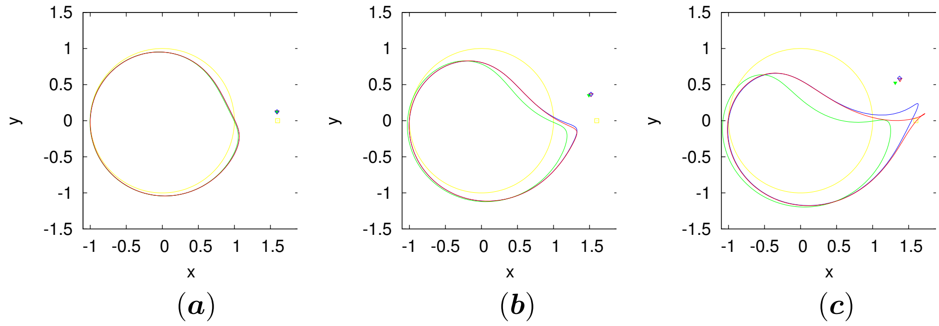

Figure 5. As in Fig. 3, but at times $t = 0.1$ a, 0.3 b, 0.5 c and for $\Gamma = 1$, $y_0 = 1.6$. Maximum errors are $3.97 \cdot 10^{-8}$, $4.41 \cdot 10^{-8}$, $4.41 \cdot 10^{-8}$.

5. Concluding remarks and future work

An analytical approach to investigate the motion of a uniform vortex in presence of a pointwise one has been built and tested by means of comparisons with contour dynamics simulations. It is found on the use of the Schwarz function of the boundary of the uniform vortex and its integral relation with the corresponding induced velocity. The solution of the resulting integrodifferential problem has been approached by evaluating its successive approximations of orders 0 and 1. The comparison with numerical simulations has been shown that the 1st order approximation behaves in a quite satisfactory way, at least for small times.

The present work is aimed to show that the numerical simulation is not the only way for investigating the planar vortex dynamics. Important, and often unexpected, information about this flow come also from the analytical handling of the strongly nonlinear equations of motion. The successive

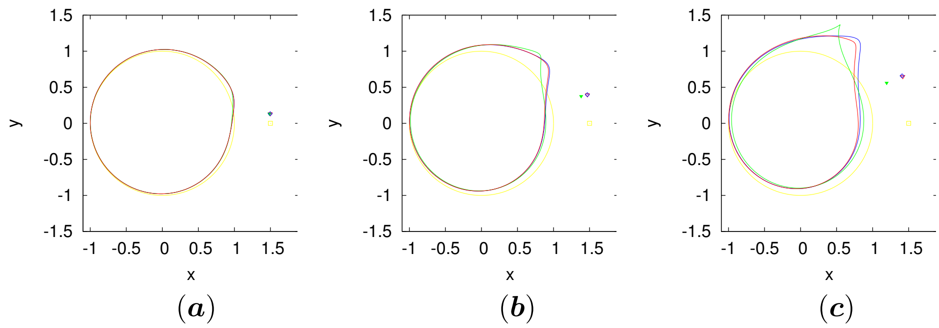

Figure 6. As in Fig. 3, but at times $t = 0.1$ (a), 0.3 (b), 0.5 (c) and for $\Gamma = -0.5$, $y_0 = 1.5$. Maximum errors are $1.85 \cdot 10^{-8}$, $1.75 \cdot 10^{-8}$ and $6.82 \cdot 10^{-9}$.

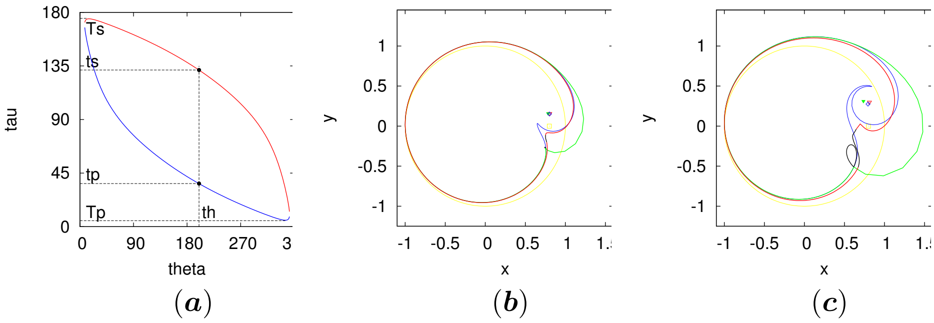

Figure 7. In $\boldsymbol{a}$, the times t'_H (blue line) and t''_H (red) are drawn vs. the argument θ of ξ, for $\Gamma = -1$ and $y_0 = 0.8$. Times and angles are in sexagesimal degrees. In $\boldsymbol{b}$ and $\boldsymbol{c}$, the snapshots of the vortices at $t = 0.1$ and 0.2 are shown. Colours and symbols are the same used in figure 3, with the only difference in using black lines to draw arcs of $\partial P^{(0,1)}$ such that the corresponding points $\xi \in \mathcal{C}$ are mapped inside $\mathcal{C}$ by the function H (11). Maximum errors in numerical simulations are $-2.30 \cdot 10^{-6}$, $1.53 \cdot 10^{-6}$ and $-1.03 \cdot 10^{-6}$.

approximations appear as a flaw of the present analysis, at least in the author opinion: a more powerful analytical approach could lead to the exact solution.

At the present time, the same approach is extended to the motion of two uniform vortices. A system of two singular nonlinear integrodifferential equations in the Schwarz functions of the boundaries is written and its analytical solution is approched by means of successive approximations. Numerical calculations show that the 1st order approximation agrees quite well with contour dynamics simulations of the motion, also in this kind of flow.

A. Necessary and sufficient condition for $\mathcal{C}_H$ intersecting $\mathcal{C}$

The present appendix investigates the position of the circle $\mathcal{C}_H$ with respect to $\mathcal{C}$. The modulus of H (11) is unitary in a point $\xi = \exp(i\,\theta) \in \mathcal{C}$ if the time t and the angle θ satisfy the trigonometric equation:

$$\underbrace{(\alpha - \beta \cos 2t)}_{c} \cos\theta + \underbrace{\beta \sin 2t}_{s} \sin\theta = \underbrace{\gamma - \delta \cos 2t}_{n}, \tag{22}$$

where $\alpha := w_0[(\Gamma+2)w_0^2 - 2]$, $\beta := w_0^3\Gamma$, $\gamma := w_0^4(\Gamma^2+2\Gamma+2)/2-1$ and $\delta := w_0^4\Gamma(\Gamma+2)/2$. The trigonometric equation in θ (22) possesses real and distinct solutions if $c^2 + s^2 > n^2$, *i.e.* if the polynomial in $\cos 2t$

$$-\delta^2\cos^2 2t - 2(\alpha\beta - \gamma\delta)\cos 2t + (\alpha^2 + \beta^2 - \gamma^2) =: P(\cos 2t)$$

is positive. In order to enforce this condition, the discriminant of P must be positive. Introduced the functions of the point vortex circulation Γ:

$$Y_+(\Gamma) := \left[1 + \left(\frac{\Gamma}{\Gamma+2}\right)^{1/2}\right]^{-1/2} \qquad \Gamma < -2 \text{ or } \Gamma > 0$$
$$Y_-(\Gamma) := \left[1 - \left(\frac{\Gamma}{\Gamma+2}\right)^{1/2}\right]^{-1/2} \qquad \Gamma > 0\,,$$

this condition is verified if $y_0 > Y_+$ for $\Gamma < -2$, for any y_0 when $-2 < \Gamma < 0$ and if $Y_+ < y_0 < Y_-$ for $\Gamma > 0$. Moreover, the roots of P are cosines of (real) angles and then they must lie in the interval $[-1, +1]$. A quite tedious discussion leads to the constraint:

$$\begin{aligned} \Gamma \le -9/4 \ &: \ Y_+ < y_0 < \sqrt{-\Gamma}+1 \\ -9/4 < \Gamma < 0 \ &: \ |\sqrt{-\Gamma}-1| < y_0 < \sqrt{-\Gamma}+1 \\ \Gamma > 0 \ &: \ Y_+ < y_0 < Y_-\,, \end{aligned} \tag{23}$$

which is necessary and sufficient for the existence of two (distinct) intersection points between the circles $\mathcal{C}_H$ and $\mathcal{C}$.

B. Trajectories of the poles Ξ_y and Ξ_w

In the present appendix the time behaviour of the poles Ξ_y and Ξ_w is investigated, with particular regard to their relative positions with respect to $\mathcal{C}$. At time t, they are the roots of the equation in ζ: $x^{(0)}(\zeta; t) = y^{(0)}(t)$. The two cases $y_0 < 1$ and $y_0 > 1$ are discussed below.

B.1. *Point vortex inside the uniform one*

The poles Ξ_y and Ξ_w are roots of the quadratic equation: $\zeta^2 - [y_0 + w_0(1 + \Gamma\,\tau)]\,\zeta + 1 = 0$, so that $\Xi_y \Xi_w = 1$. They are:

$$\Xi_{y,w} = \frac{y_0 + w_0}{2} + \frac{\Gamma w_0}{2}\left[\tau \mp \sqrt{(\tau - \tau_1^\star)(\tau - \tau_2^\star)}\right]\ , \tag{24}$$

the branch points belonging to the real axis: $\tau_{1,2}^\star = -(1 \mp y_0)^2/\Gamma$. The complexified time τ runs (clockwise) on the circle $\mathcal{C}_1$ with radius $1/2$ and center in $1/2$, by starting form the origin at $t = 0$ and crossing the real axis in the point 1 at $t = \pi/2$. As a consequence, it is important to order the above branch points and to point out their relative positions with respect to 1. This is made in figure 8-a for any Γ and y_0. In the case in which the branch cut of the square root (24) includes the point 1, the trajectories of the poles jump at $t = \pi/2$, as shown in figure 8-b.

B.2. *Point vortex outside the uniform one*

The poles are the roots of the quadratic equation in ζ: $\zeta^2 - \{y_0 + w_0 + [\Gamma w_0 - 2(y_0 - w_0)]\tau\}\zeta + [1 - 2(1 - w_0^2)\tau] = 0$. Named as a and b the coefficients of ζ^1 and ζ^0, $|b| = 1$ just at $t = 0$ (or $t = \pi$), while $|b| < 1$ at the other times. The above equation is rewritten in terms of the new unknown $\zeta' := \zeta/\sqrt{b}$ as $\zeta'^2 + (a/\sqrt{b})\,\zeta' + 1 = 0$. As it occurs in the previous case, the roots $\Xi'_{y,w}$ of that equation can be defined in such a way that one lies inside the unit circle (Ξ'_w) and the other (Ξ'_y) is external. It follows that $\Xi_w = \sqrt{b}\,\Xi'_w$, is always internal to $\mathcal{C}$, while the other $\Xi_y = \sqrt{b}\,\Xi'_y$ can lie outside or inside the same circle. The necessary and sufficient condition for Ξ_y crossing $\mathcal{C}$ is investigated, but it will not be discussed here, for shortness.

Once the singular ($\Gamma_p := 2(y_0^2 - 1)$) and the branch ($\Gamma_b := 2(y_0 - w_0)^2$) circulations have been defined, the poles are written for $\Gamma \neq \Gamma_p$ as:

$$\Xi_{y,w} = \frac{1}{2}\left\{ (y_0 + w_0) + w_0(\Gamma - \Gamma_p)\left[\tau \pm \sigma\sqrt{(\tau - \tau_1^\star)(\tau - \tau_2^\star)}\right]\right\} \tag{25}$$

where $\sigma := \mathrm{sign}(\Gamma - \Gamma_p)$ and $\tau_{1,2}^\star = -y_0^2\{\Gamma - \Gamma_b + w_0^2\Gamma \pm 2w_0[\Gamma(\Gamma - \Gamma_b)]^{1/2}\}/(\Gamma - \Gamma_p)^2$, while special formulae must be employed for $\Gamma = \Gamma_p$. Figure 9 shows the different kinds of trajectories of the poles (25), for sample values of y_0 and Γ.

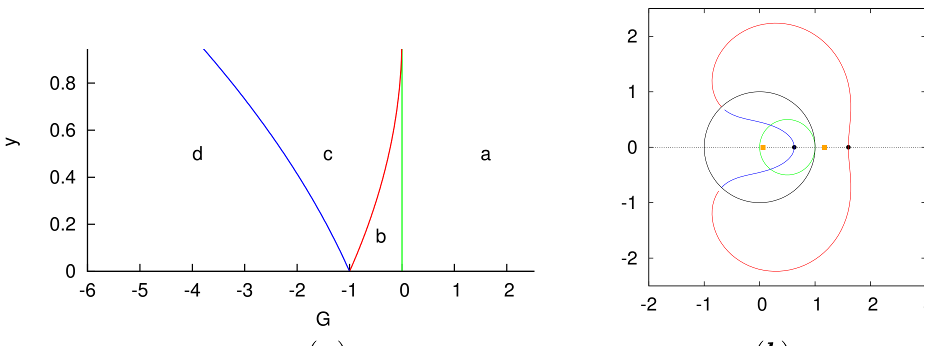

(a) (b)

Figure 8. In (a) the relative positions of the branch points $\tau_{1,2}^\star$ are defined in the plane (Γ, y_0): a: $\tau_2^\star < \tau_1^\star < 0$; b: $1 < \tau_1^\star < \tau_2^\star$; c: $0 < \tau_1^\star < 1 < \tau_2^\star$; d: $0 < \tau_1^\star < \tau_2^\star < 1$. Red and blue curves are defined by the equations: $y_0 = 1 - \sqrt{-\Gamma}$ and $y_0 = \sqrt{-\Gamma} - 1$, respectively. In (b) the trajectories of the poles Ξ_y (blue) and Ξ_w (red) are drawn for $\Gamma = -9/4$, $y_0 = 5/8$. In the picture the τ-plane (the circle $\mathcal{C}_1$ on which τ runs is drawn with a green line and the branch points $\tau_{1,2}^\star$ with orange symbols) and the ξ-plane ($\mathcal{C}$ is drawn with a black line and the points y_0, w_0 with black symbols) are superimposed.

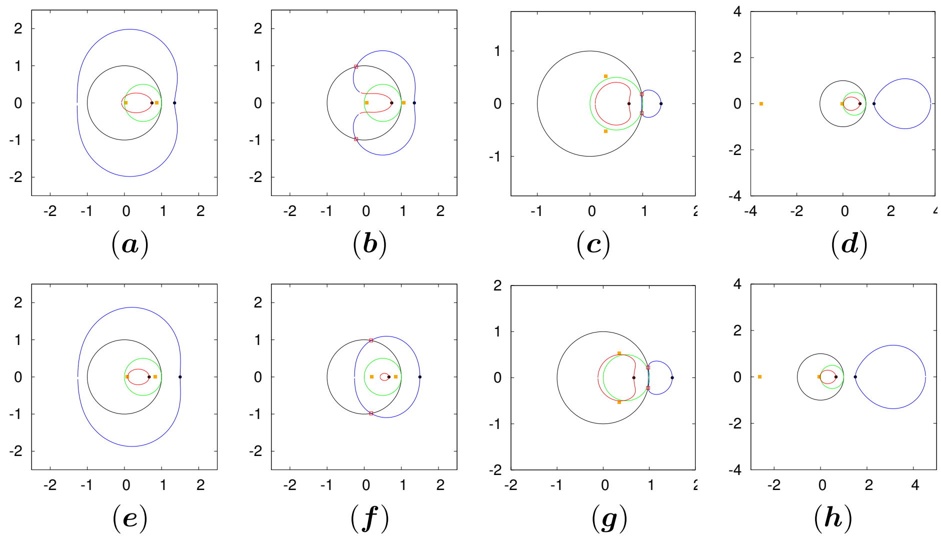

Figure 9. Samples of trajectories of the poles (25) Ξ_y (blue) and Ξ_w (red) are drawn for $t \in [0, \pi)$. The points y_0 and w_0 are drawn with black filled circles, the branch points $\tau^\star_{1,2}$ with orange filled squares and the points in which the curve Ξ_y crosses $\mathcal{C}$ with empty red squares. The initial position of the point vortex is fixed to $y_0 = 1.35$ in the first row and to $y_0 = 1.5$ in the second one, while the circulation Γ takes the following values: a: -3, b: $-3/2$, c: 0.28, d: 4, e: $-5/2$, f: $-1/2$, g: 0.55, h: 6.

REFERENCES

1. E. A. Overman and N. J. Zabusky, Evolution and merger of isolated vortex structures, *Physics of Fluids*, vol. 25, no. 8, pp. 1297–1305, 1982.
2. N. J. Z. M. V. Melander and A. S. Styczek, A moment model for vortex interactions of the two-dimensional euler equations. Part 1. Computational validation of a hamiltonian elliptical representation, *Journal of Fluid Mechanics*, vol. 167, pp. 95–115, 1986.
3. N. J. Z. M. V. Melander and J. C. McWilliams, Asymmetric vortex merger in two-dimensions: Which vortex is victorious?, *Physics of Fluids*, vol. 30, no. 9, pp. 2610–2612, 1987.
4. R. W. Griffiths and E. J. Hopfinger, Coalescence of geostrophic vortices, *Journal of Fluid Mechanics*, vol. 178, pp. 975–980, 1987.
5. D. G. Dritschel, Contour dynamics and contour surgery: numerical algorithms for extended,high-resolution modelling of vortex dynamics in two-dimensional, inviscid, incompressible flows, *Computer Physics Report*, vol. 10, no. 77–146, 1989.
6. D. G. Dritschel and D. W. Waugh, Quantification of the inelastic interaction of unequal vortices in two-dimensional vortex dynamics, *Physics*

of Fluids A, vol. 4, no. 8, pp. 1737–1744, 1992.

7. I. Yasuda and G. R. Flierl, Two-dimensional asymmetric vortex merger: contour dynamics experiment, *Journal of Oceanography*, vol. 51, no. 2, pp. 145–170, 1995.
8. M. Amoretti, D. Durkin, J. Fajans, R. Pozzoli, and M. Romé, Experimental and numerical study of asymmetric vortex merger in a pure electron plasma, in *Non-neutral Plasma Physics IV* (F. Anderegg, L. Schweikhard, C. F. Driscoll, and J. A. Christina, eds.), pp. 459–463, Melville, NY: American Institute of Physics, 2002.
9. L. K. Brandt and K. K. Nomura, Characterization of the interactions of two unequal co-rotating vortices, *Journal of Fluid Mechanics*, vol. 646, pp. 233–253, 2010.
10. F. Jing, E. Kanso, and P. K. Newton, Insights into symmetric and asymmetric vortex mergers using the core growth model, *Physics of Fluids*, vol. 24, no. 073101, 2012.
11. D. Z. Jin and D. H. E. Dubin, Point vortex dynamics within a background vorticity patch, *Physics of Fluids*, vol. 13, no. 3, pp. 677–691, 2001.
12. D. Durkin and F. Fajans, Experimental dynamics of a vortex within a vortex, *Physical Review Letters*, vol. 85, no. 19, pp. 4052–4055, 2000.
13. G. Riccardi, Intrinsic dynamics of the boundary of a two-dimensional uniform vortex, *Journal of Engineering Mathematics*, vol. 50, no. 1, pp. 51–74, 2004.
14. G. Riccardi, Toward analytical contour dynamics, in *Applied and Industrial Mathematics in Italy III* (E. D. Bernardis, R. Spigler, and V. Valente, eds.), pp. 496–507, Singapore: World Scientific, 2009.
15. G. Riccardi, An analytical study of the self-induced inviscid dynamics of two-dimensional uniform vortices, *Acta Mechanica*, vol. 224, no. 2, pp. 307–326, 2013.
16. G. Riccardi and D. Durante, Velocity induced by a plane uniform vortex having the Schwarz function of its boundary with two simple poles, *Journal of Applied Mathematics, Hindawi Publications*, 2008.
17. P. J. Davis, *The Schwarz function and its applications.* Cambridge: Cambridge University Press, 6th ed., 1932.
18. H. T. Davis, *Introduction to nonlinear differential and integral equations.* New York: Dover, 1962.
19. F. G. Tricomi, *Integral equations.* New York: Dover, 1985.
20. M. J. Ablowitz and A. S. Fokas, *Complex Variables (Introduction and Applications).* Cambridge: Cambridge University Press, second ed., 2003.